Supporting Information

A unique space confined strategy to construct defective metal oxides within porous nanofibers for electrocatalysis

Qi Hu[#], Ziyu Wang[#], Xiaowan Huang, Yongjie Qin, Hengpan Yang, Xiangzhong Ren, Qianling Zhang, Jianhong Liu, Chuanxin He

Experimental Section

Synthesis of D-CoNiO$_x$-NFs

The CoNi-PBAs cubes were synthesized in advance according to literatures. The CoNi-PBAs were then employed as precursors to craft D-CoNiO$_x$-NFs via an electrospinning technology. In a typical process, 1.0 g polyacrylonitrile (PAN, Mw=150000 g mol^{-1}) was completely dissolved in 14 ml *N,N*-dimethylformamide (DMF) under vigorously stirring for 24 h, in which CoNi-PBAs (1.0 g) was added to form a suspension. The obtained suspension was then poured into a syringe with a stainless steel needle at an applied voltage of 18 kV for implementing the electrospinning process. The resulting membranes were dried in vacuum for 12 h, and pre-oxidized at 280 ^{o}C for 3 h under air atmosphere. After that, the membranes were calcinated at 500 ^{o}C for 2 h to remove the PAN, and the obtained product was denoted

D-$CoNiO_x$-NFs. For comparison, we utilized a certain amount of $Ni(NO_3)_2$ and $Co(NO_3)_2$ to replace CoNi-PBAs without changing the mole fraction of Ni/Co cations in the spinning solution, repeated the above steps, and then obtained $CoNiO_x$-NFs (served as control samples).

Synthesis of D-$CoNiO_x$-P-NFs

The P elements were doped into D-$CoNiO_x$-NFs to generate D-$CoNiO_x$-P-NFs by employing sodium hypophosphite (NaH_2PO_2) as P sources. In details, D-$CoNiO_x$-NFs (0.2 g) and NaH_2PO_2 (2.4 g) were put into two separated sides of a crucible, which was then calcinated at 250 ^oC under Ar atmosphere for 0.5 h. In order to optimize the content of P dopants, we altered the amount of NaH_2PO_2 introduced from 1.2 to 0.8 and 1.6 g for crafting control samples of D-$CoNiO_x$-2P-NFs and D-$CoNiO_x$-4P-NFs, respectively. For comparison, we also introduced P dopants into $CoNiO_x$-NFs through the same process for the synthesis of D-$CoNiO_x$-P-NFs, and the obtained product was denoted $CoNiO_x$-P-NFs.

Characterization

Crystalline phases of all samples were identified through X-ray diffraction (XRD) experiments at a 2θ range of 10°-80° (D8ADVANCE diffractometer). Morphological properties of the samples were viewed by field emission scanning electron microscope (FESEM) (JEOL JEM-7800F), transmission electron microscopy (TEM)

(JEOL JEM 2100) and high-resolution transmission electron microscopy (HRTEM) (JEOL JEM-F200) with SADE spectrum. Chemical states of different elements were analyzed via X-ray photoelectron spectroscopy (XPS) using a Thermo VG ESCALAB250 X-ray photoelectron spectrometer. The low-temperature N_2 adsorption-desorption tests were performed on a micromeritics ASAP 2020 sorptemeter. X-ray absorption fine structure spectroscopy (XAFS) of Co K-edge and Ni K-edge were recorded at 1W1B station in Beijing Synchrotron Radiation Facility (BSRF). The storage rings of BSRF was operated at 2.5 GeV with a maximum current of 250 mA. All XAFS data was collected in a transmission mode using ionization chamber under ambient conditions.

Electrochemical measurements

All electrochemical measurements were performed on an electrochemical workstation (CHI 760 E) using a three-electrode system that contains a Hg/HgO (in 1 M KOH) as reference electrode, a carbon rod as counter electrode, and a glassy carbon electrode (0.07 cm^2) as working electrode. OER and HER were performed under O_2- and Ar-saturated 1 M KOH, respectively. All LSVs were recorded at a scan rate of 5 mV s^{-1}. The electrocatalysts inks were prepared through dispersing a certain amount of electrocatalysts in a mixed solution of ethanol (49 μL), deionized water (150 μL), and Nafion (9 μL) under a sonication bath for 30 min. The potentials of all LSV were converted into a reversible hydrogen electrode (RHE) according to the equation: "E (RHE)= E (Hg/HgO) + 0.098 + 0.059 × pH. All potentials were

recorded after being calibrated IR-compensations. Electrochemical impedance spectroscopy (EIS) were tested over a frequency range from 1 MHz to 1 Hz. According to cyclic voltammetry (CV) sweeps over a faraday current-free region at various scan rates, we determined the electrochemically active surface area (ECSA) of different samples. The Tafel plots were drawn through fitting the linear range of the overpotential (η) and log current densities (log j), based on the equation of η = b log(j) + a, where b is the Tafel slope

The overall water-splitting performance was measured on a two-electrode system by serving the nickel foams with electrocatalysts (mass loading: 1 mg cm^{-2}) as both cathode and anode. The overall water splitting durability was accessed by recording the current density at a constant voltage for 20 h.

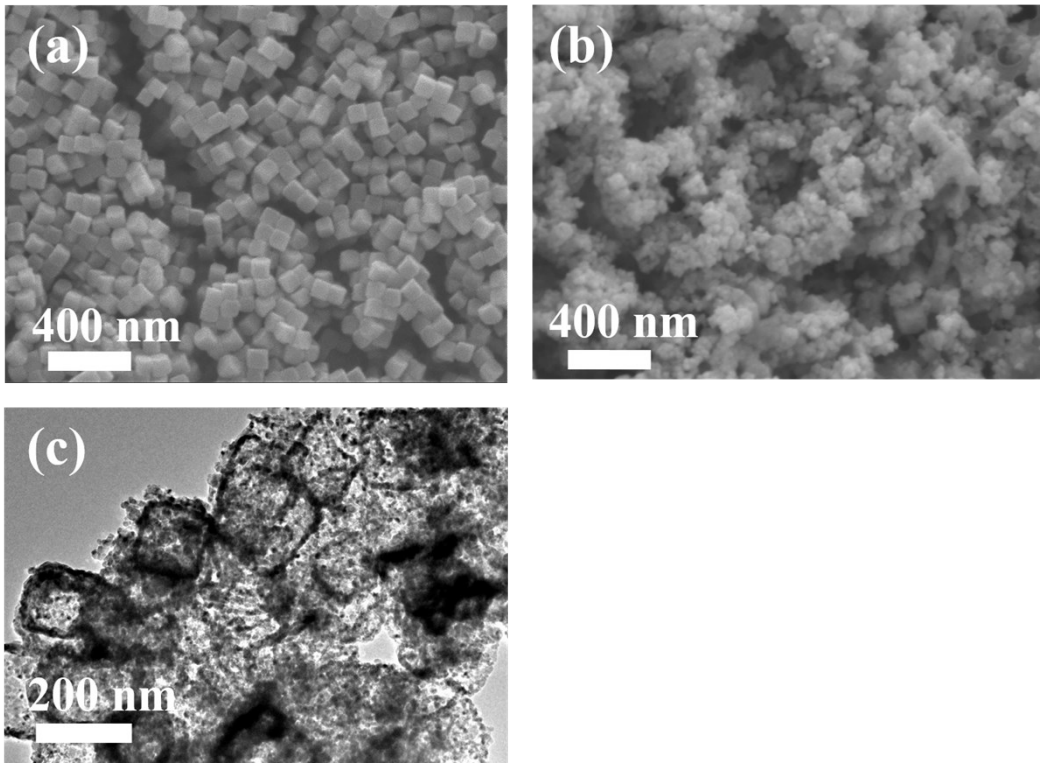

Figure S1 (a) SEM images of pure CoNi-PBAs cubes with PAN. (b) SEM and (c) TEM images of CoNi-PBAs cubes after the calcination at 500 ^{o}C in air for 2 h.

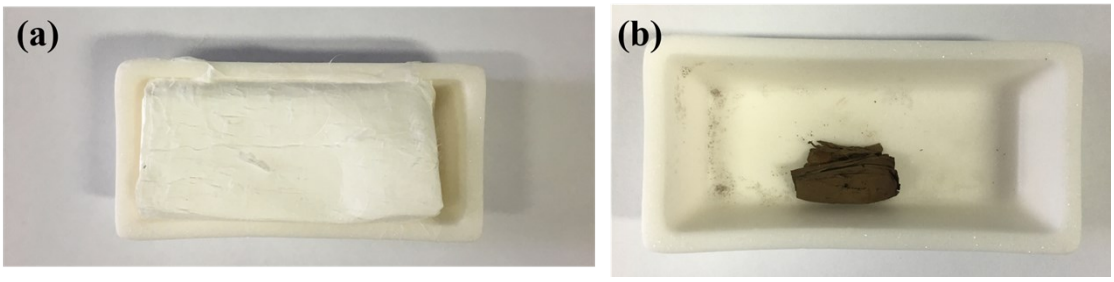

Figure S2 Optical photos of pure PAN nanofiber membrane without CoNi-PBAs (a) before and (b) after the calcination at 500 ^{o}C in air for a short time of 0.5 h.

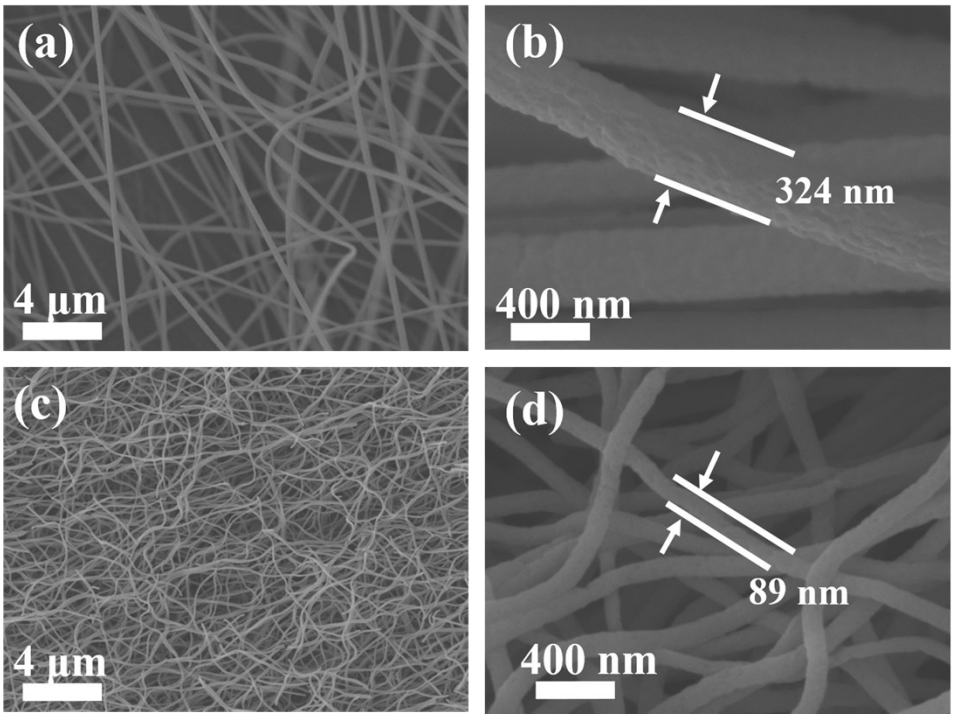

Figure S3 SEM images pure PAN nanofiber membrane (a, b) before and (c, d) after the calcination at 500 ^{o}C in air for a short time of 0.5 h.

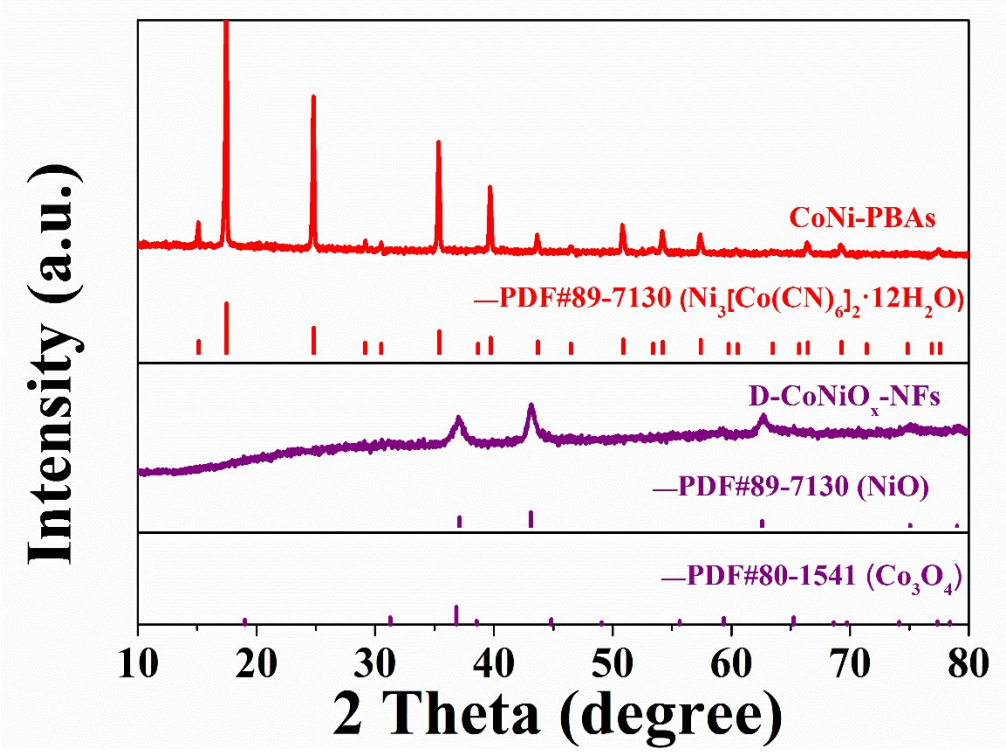

Figure S4 XRD patterns of CoNi-PBAs and D-CoNiO_x-NFs.

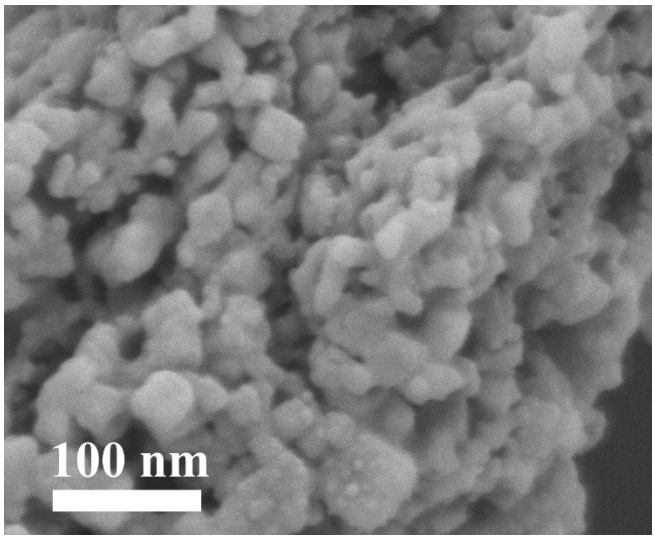

Figure S5 SEM images of D-CoNiO_x-NFs, which was prepared through the calcination of CoNi-PBAs@PAN-NFs at 500 °C in air for 2 h.

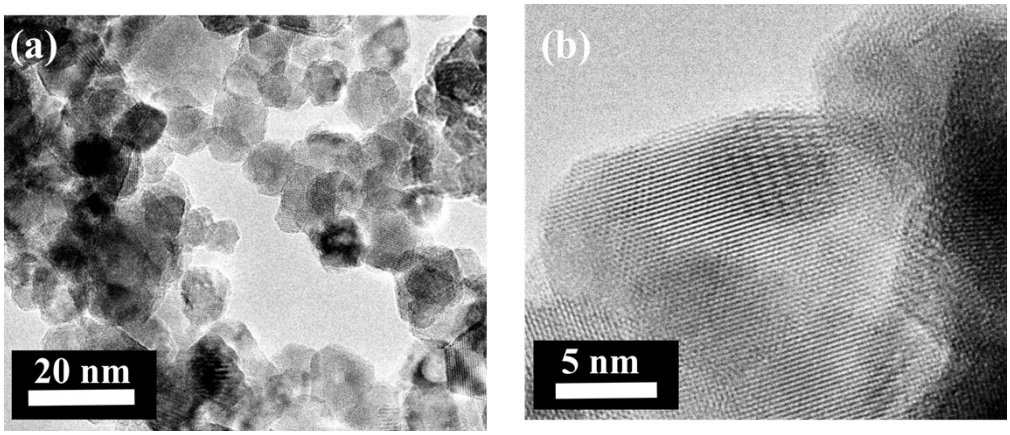

Figure S6 (a) TEM and (b) HRTEM images of $CoNiO_x$, which was synthesized pure CoNi-PBAs without PAN.

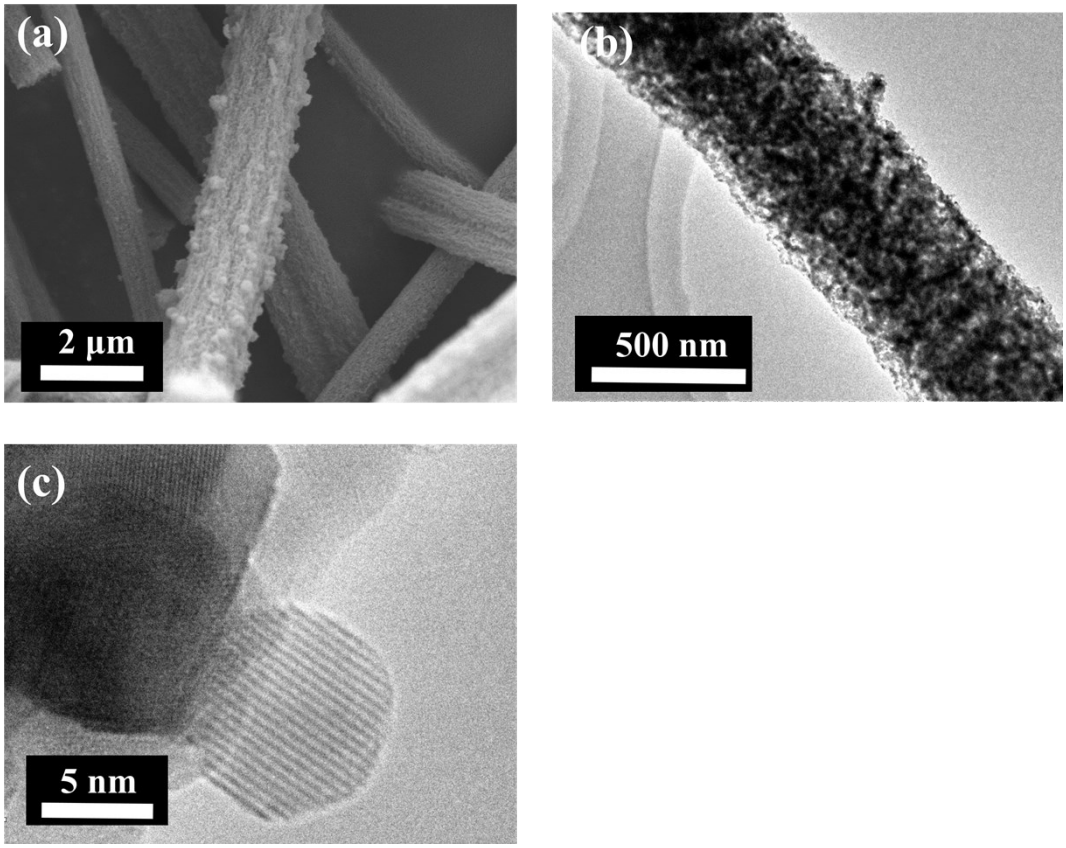

Figure S7 (a) SEM, (b) TEM, and (c) HRTEM images of $CoNiO_x$-NFs.

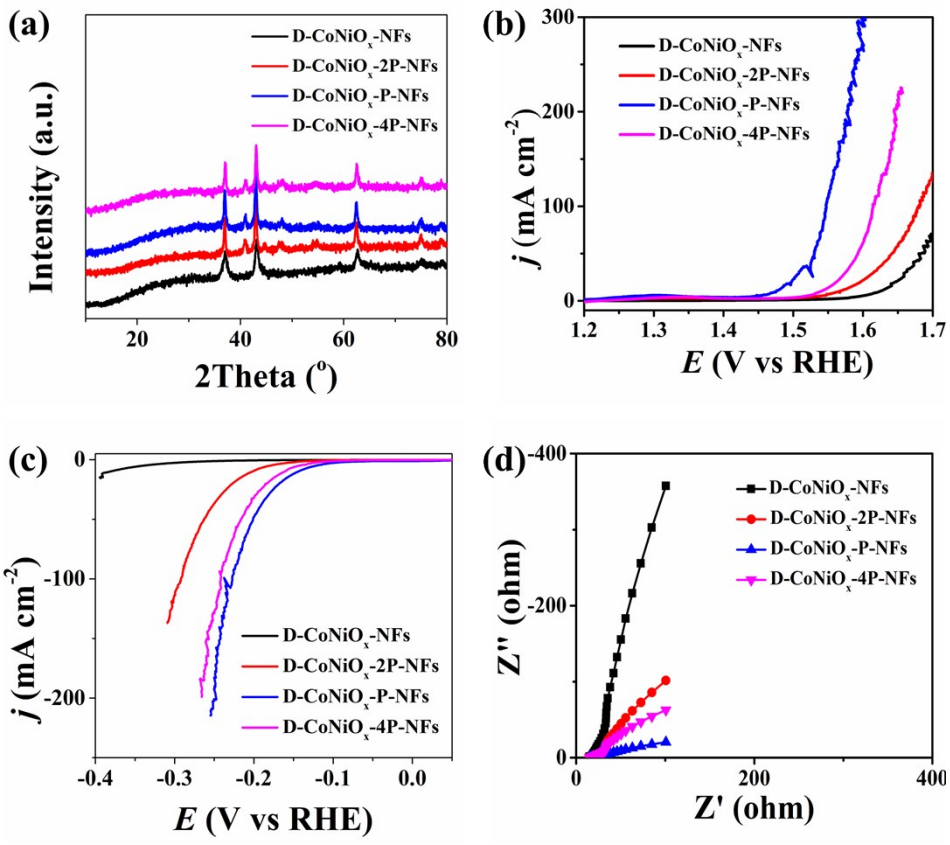

Figure S8 (a) XRD patterns of D-CoNiO$_x$-NFs, D-CoNiO$_x$-2P-NFs, D-CoNiO$_x$-P-NFs, and D-CoNiO$_x$-4P-NFs with different amount of P dopants. LSV of (b) OER and (c) HER for above noted four electrocatalysts. (d) EIS Nyquist plots of electrocatalysts for OER at the overpotential of 300 mV.

$H_2O + e^- \rightarrow H^* + OH^-$ Volmer step, Tafel slope = 120 mV dec^{-1}

$H^* + H_2O + e^- \rightarrow H_2 + OH^-$ Heyrovsky step, Tafel slope = 40 mV dec^{-1}

$H^* + H^* \rightarrow H_2$ Tafel step, Tafel slope = 30 mV dec^{-1}

Figure S9 Reaction processes of HER in alkaline media, and Tafel slope values for every step of HER.[S1]

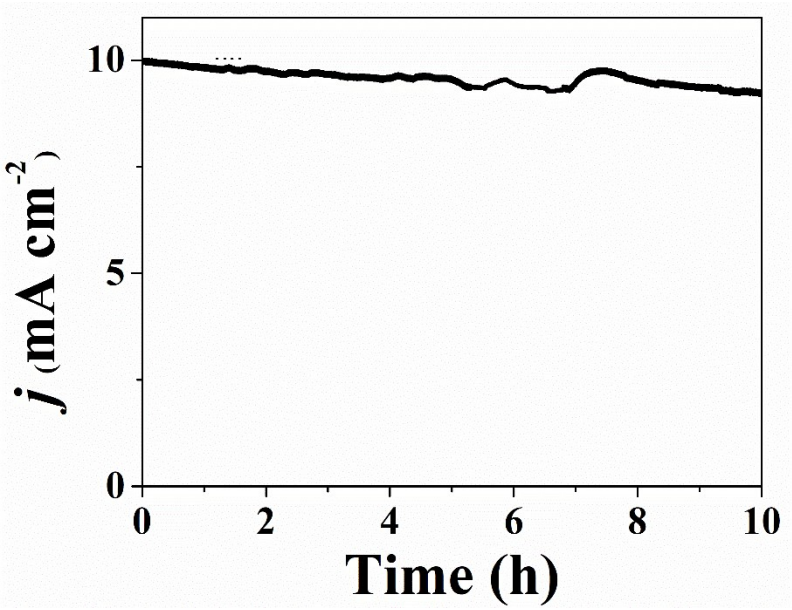

Figure S10 Stability test of D-CoNiO$_x$-P-NFs for OER at 10 mA cm^{-2}.

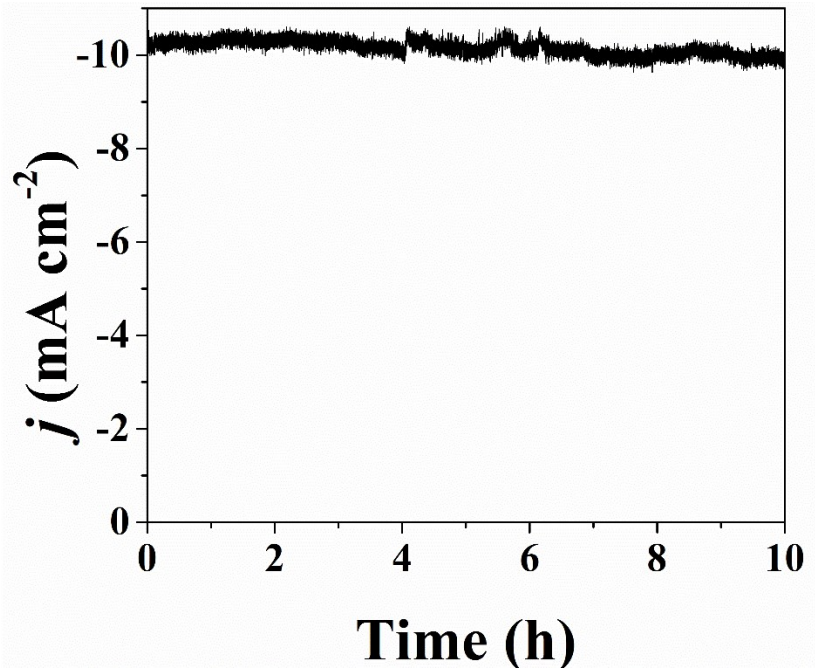

Figure S11 Stability test of D-CoNiO$_x$-P-NFs for HER at 10 mA cm^{-2}.

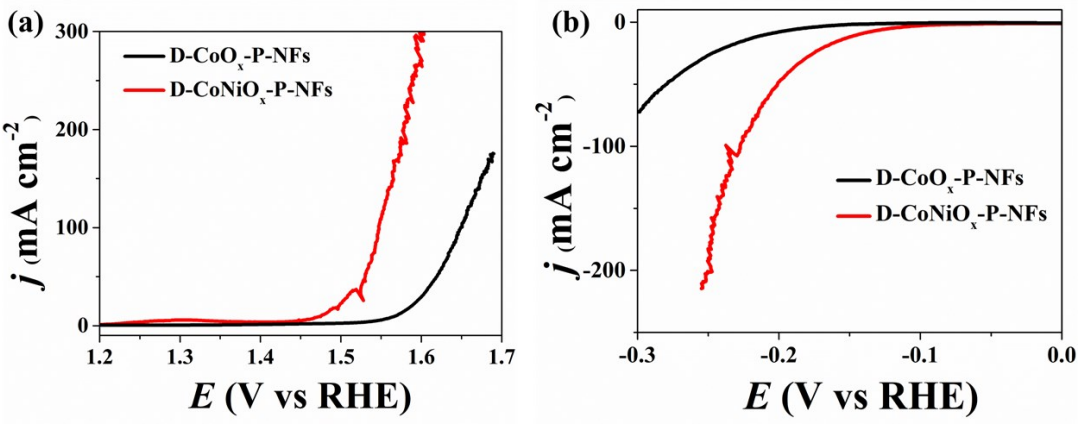

Figure S12 LSV profiles of D-CoO_x-P-NFs and D-$CoNiO_x$-P-NFs for (a) OER and (b) HER in 1 M KOH

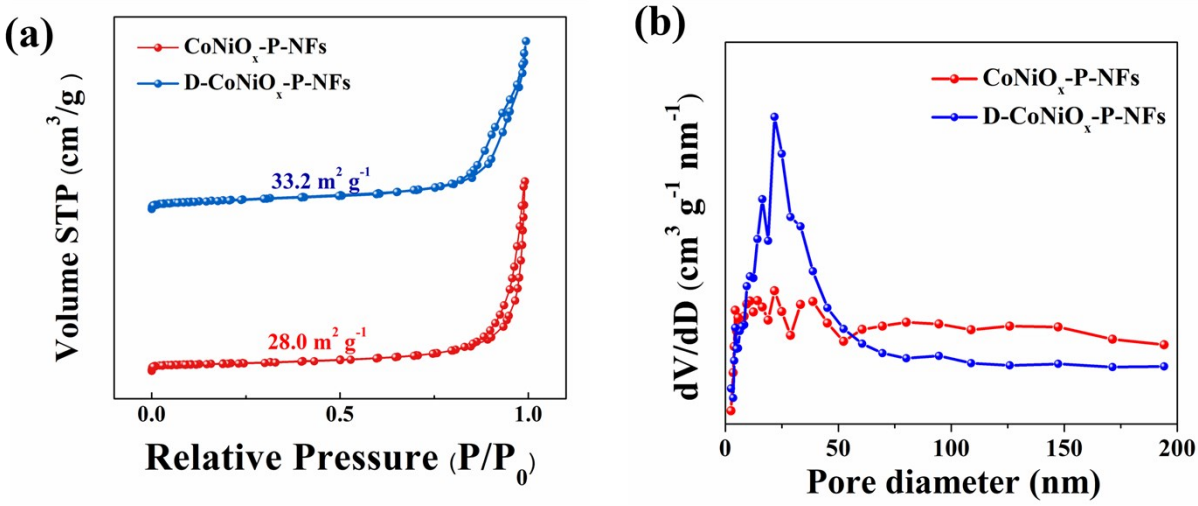

Figure S13 (a) N_2 adsorption-desorption isotherms and corresponding pore distribution of $CoNiO_x$-P-NFs and D- $CoNiO_x$-P-NFs.

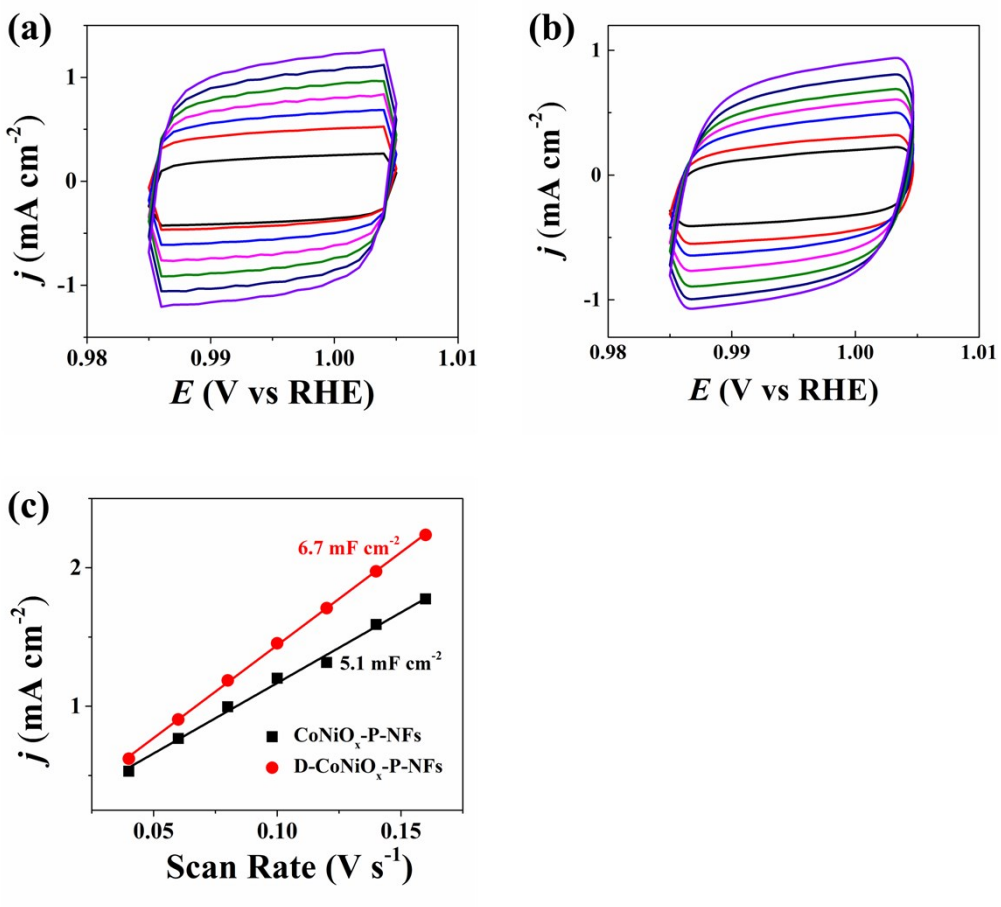

Figure S14 CV profiles for (a) $CoNiO_x$-P-NFs, (b) D-$CoNiO_x$-P-NFs. (c) Current density *vs* scan rate plots for $CoNiO_x$-P-NFs, and D-$CoNiO_x$-P-NFs at different scan rates.

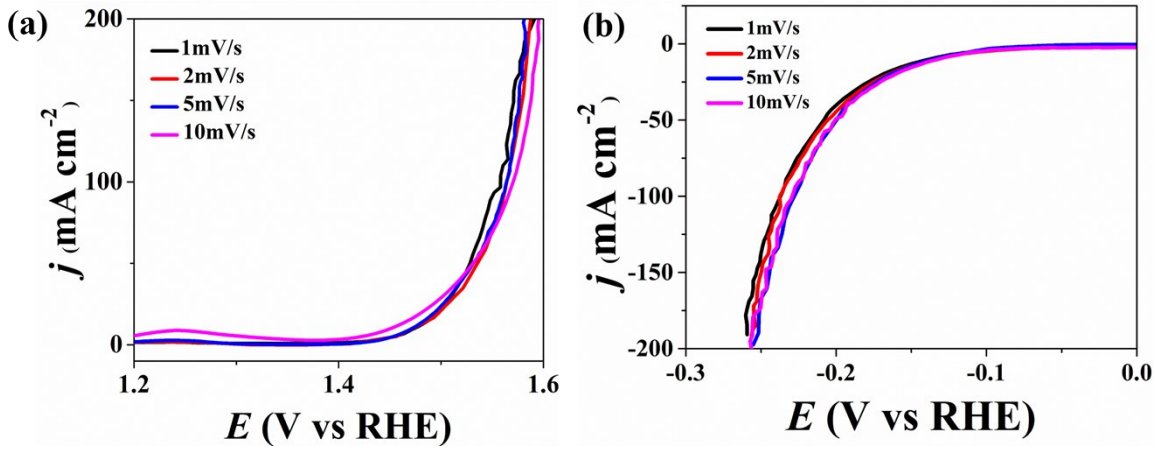

Figure S15 LSV profiles of D-$CoNiO_x$-P-NFs for (a) OER and (b) HER at different scan rates in 1 M KOH

Figure S16 LSV of (a) OER and (b) HER for $CoNiO_x$-P-NFs and D- $CoNiO_x$-P-NFs after normalizing by ECSA.

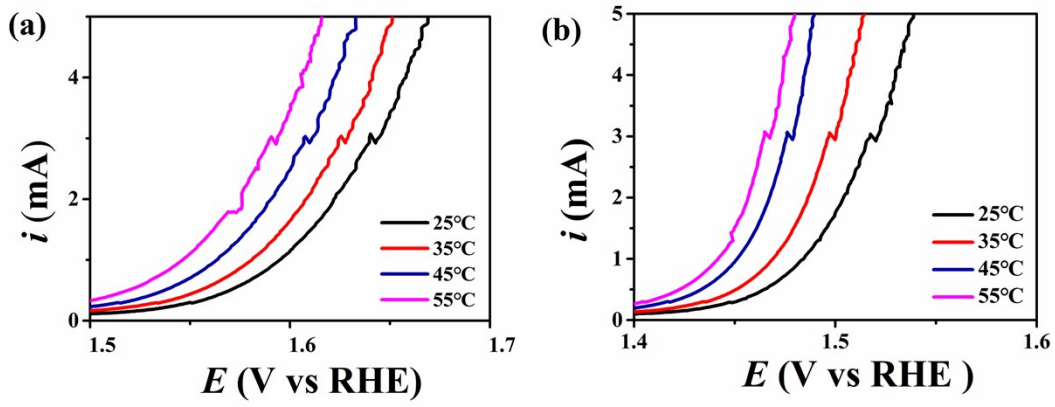

Figure S17 LSV of OER for (a) $CoNiO_x$-P-NFs, (b) D-$CoNiO_x$-P-NFs at different temperatures from 25 to 55 °C.

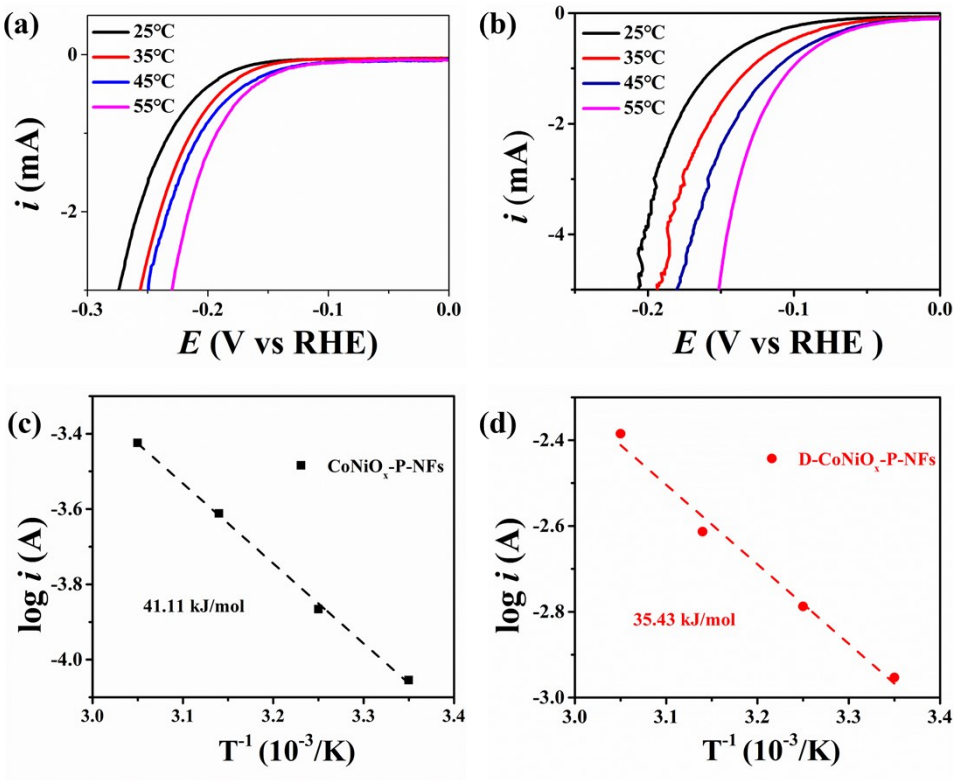

Figure S18 LSV of HER for (a) $CoNiO_x$-P-NFs, and (b) D-$CoNiO_x$-P-NFs at different temperatures from 25 to 55 °C. Arrhenius plots of the HER kinetic current on (c) $CoNiO_x$-P-NFs, and (d) D-$CoNiO_x$-P-NFs at the overpotential of 150 mV.

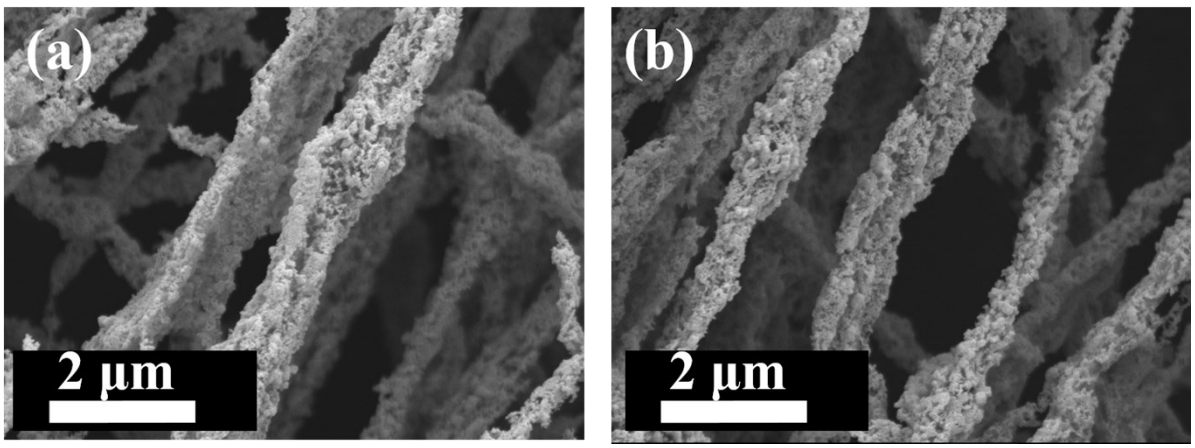

Figure S19 SEM images D-$CoNiO_x$-P-NFs after (a) OER stability and (b) HER stability test.

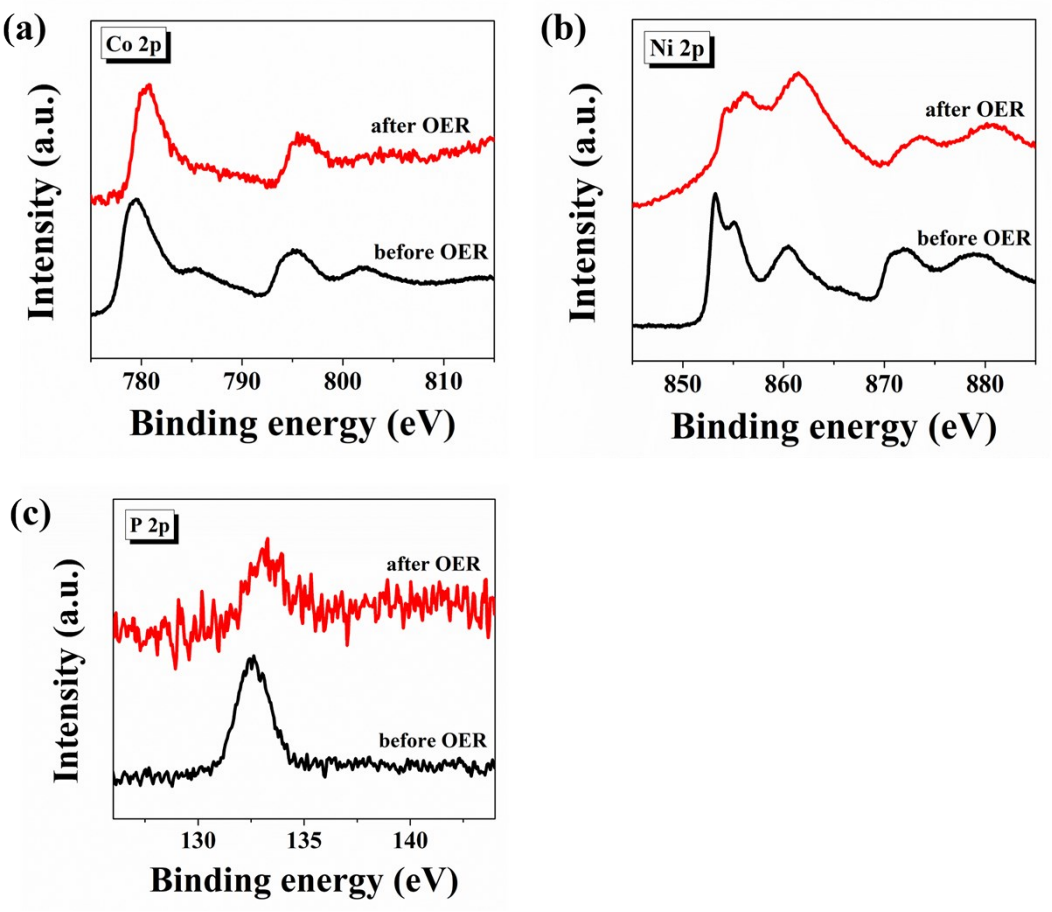

Figure S20 XPS spectra of (a) Co 2p, (b) Ni 2p, and (c) P 2p for D-CoNiO_x-P-NFs after OER stability tests.

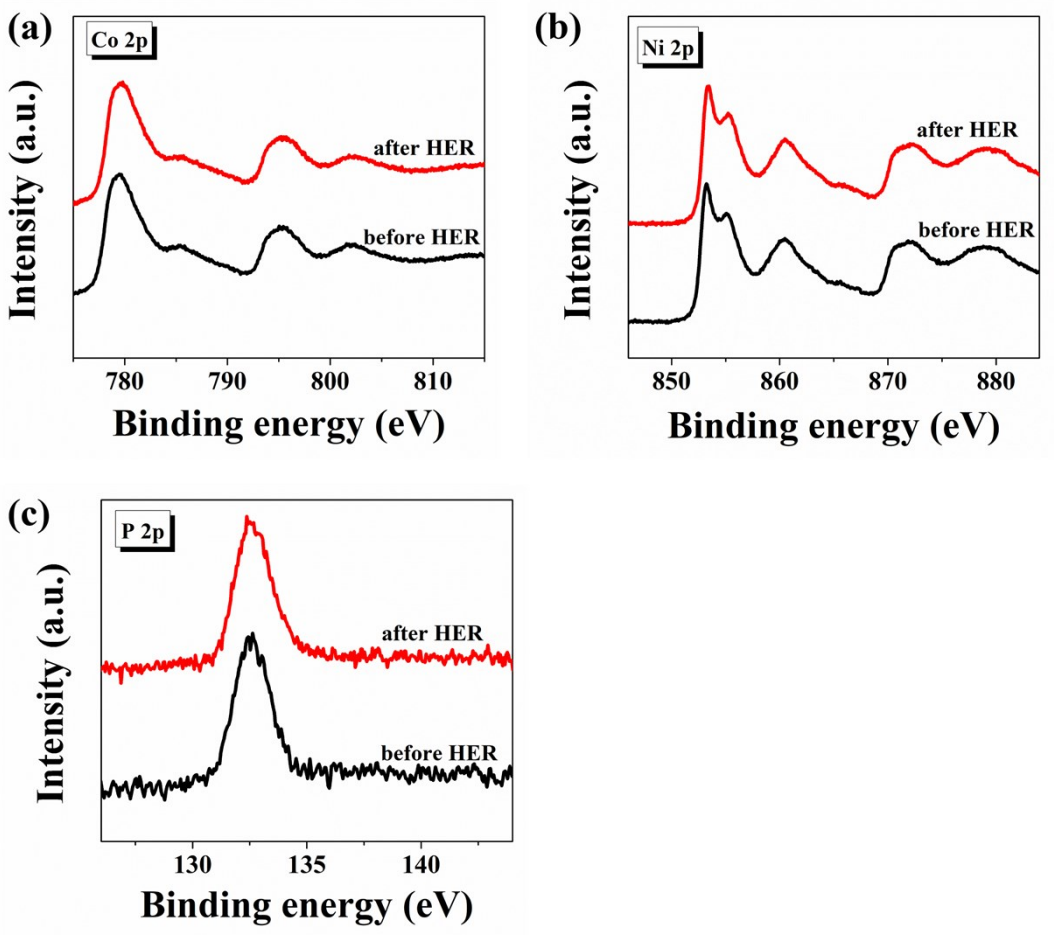

Figure S21 XPS spectra of (a) Co 2p, (b) Ni 2p, and (c) P 2p for D-CoNiO$_x$-P-NFs after HER stability tests.

References

[S1] S. Ye, F. Luo, T. Xu, P. Zhang, H. Shi, S. Qin, J. Wu, C. He, X. Ouyang, Q. Zhang, J. Liu, X. Sun, *Nano Energy* **2020**, *68*, 104301.